

Čerenkov Particle Identification in FOCUS

The FOCUS Collaboration

J.M. Link^a, M. Reyes^{a,2}, P.M. Yager^a, J.C. Anjos^b,
I. Bediaga^b, C. Göbel^{b,3}, J. Magnin^b, A. Massafferri^b,
J.M. de Miranda^b, I.M. Pepe^{b,4}, A.C. dos Reis^b, S. Carrillo^c,
E. Casimiro^{c,5}, E. Cuautle^{c,1}, A. Sánchez-Hernández^c,
C. Uribe^{c,6}, F. Vazquez^c, L. Cinquini^{d,7}, J.P. Cumalat^d,
B. O'Reilly^d, J.E. Ramirez^d, E.W. Vaandering^{d,8}, J.N. Butler^e,
H.W.K. Cheung^e, I. Gaines^e, P.H. Garbincius^e, L.A. Garren^e,
E. Gottschalk^e, P.H. Kasper^e, A.E. Kreymer^e, R. Kutschke^e,
S. Bianco^f, F.L. Fabbri^f, S. Sarwar^f, A. Zallo^f, C. Cawfield^g,
D.Y. Kim^g, K.S. Park^{g,9}, A. Rahimi^{g,17}, J. Wiss^g,
R. Gardner^h, A. Kryemadhi^h, Y.S. Chungⁱ, J.S. Kangⁱ,
B.R. Koⁱ, J.W. Kwakⁱ, K.B. Lee^{i,10}, H. Park^{i,11}, G. Alimonti^j,
M. Boschini^j, P. D'Angelo^j, M. DiCorato^j, P. Dini^j,
M. Giammarchi^j, P. Inzani^j, F. Leveraro^j, S. Malvezzi^j,
D. Menasce^j, M. Mezzadri^j, L. Milazzo^j, L. Moroni^j,
D. Pedrini^j, C. Pontoglio^j, F. Prelz^j, M. Rovere^j, S. Sala^j,
T.F. Davenport III^k, L. Agostino^{l,12}, V. Arena^l, G. Boca^l,
G. Bonomi^{l,13}, G. Gianini^l, G. Liguori^l, M.M. Merlo^l,
D. Pantea^{l,14}, S.P. Ratti^l, C. Riccardi^l, I. Segoni^{l,12},
P. Vitulo^l, H. Hernandez^m, A.M. Lopez^m, H. Mendez^m,
L. Mendez^m, E. Montiel^m, D. Olaya^{m,12}, A. Paris^m,
J. Quinones^m, C. Rivera^m, W. Xiong^m, Y. Zhang^{m,15},
J.R. Wilsonⁿ, K. Cho^{o,11}, T. Handler^o, R. Mitchell^o,

arXiv:hep-ex/0108011v1 6 Aug 2001

D. Engh^p, W.E. Johns^p, M. Hosack^p, M.S. Nehring^{p,16},
P.D. Sheldon^p, K. Stenson^p, M.S. Webster^p, M. Sheaff^q

- ^a*University of California, Davis, CA 95616*
- ^b*Centro Brasileiro de Pesquisas Físicas, Rio de Janeiro, RJ, Brazil*
- ^c*CINVESTAV, 07000 México City, DF, Mexico*
- ^d*University of Colorado, Boulder, CO 80309*
- ^e*Fermi National Accelerator Laboratory, Batavia, IL 60510*
- ^f*Laboratori Nazionali di Frascati dell'INFN, Frascati, Italy, I-00044*
- ^g*University of Illinois, Urbana-Champaign, IL 61801*
- ^h*Indiana University, Bloomington, IN 47405*
- ⁱ*Korea University, Seoul, Korea 136-701*
- ^j*INFN and University of Milano, Milano, Italy*
- ^k*University of North Carolina, Asheville, NC 28804*
- ^l*Dipartimento di Fisica Nucleare e Teorica and INFN, Pavia, Italy*
- ^m*University of Puerto Rico, Mayaguez, PR 00681*
- ⁿ*University of South Carolina, Columbia, SC 29208*
- ^o*University of Tennessee, Knoxville, TN 37996*
- ^p*Vanderbilt University, Nashville, TN 37235*
- ^q*University of Wisconsin, Madison, WI 53706*

Abstract

We describe the algorithm used to identify charged tracks in the fixed-target charm-photonproduction experiment FOCUS. We begin by describing the new algorithm and contrast this approach with that used in our preceding experiment—E687. We next illustrate the algorithm's performance using physics signals. Finally we briefly describe some of the methods used to monitor the quantum efficiency and noise of the Čerenkov cells.

1 Introduction

FOCUS is a fixed-target experiment concentrating on the photoproduction of charm that accumulated data at Fermilab from 1996–1997. It is a considerably upgraded version of a previous experiment, E687 [1]. In FOCUS, a forward multi-particle spectrometer is used to measure the interactions of high energy photons on a segmented BeO target. We obtained a sample of over 1 million fully reconstructed charm particles in the three major decay modes: $D^0 \rightarrow K^-\pi^+$, $K^-\pi^+\pi^-\pi^+$, and $D^+ \rightarrow K^-\pi^+\pi^+$ (and charge conjugates). We will refer to these as “golden modes”.

¹ Present Address: Instituto de Ciencias Nucleares, Universidad Nacional Autónoma de México. CP 04510. México

² Present Address: Instituto de Física y Matemáticas, Universidad Michoacana de San Nicolás de Hidalgo, Morelia, Mich., Mexico 58040

³ Present Address: Instituto de Física, Facultad de Ingeniería, Univ. de la República, Montevideo, Uruguay

⁴ Present Address: Instituto de Física, Universidade Federal da Bahia, Salvador, Brazil

⁵ Present Address: INFN sezione di Milano, Milano, Italy

⁶ Present Address: Instituto de Física, Universidad Autónoma de Puebla, Puebla, México

⁷ Present Address: National Center for Atmospheric Research, Boulder, CO

⁸ Present Address: Vanderbilt University, Nashville, TN 37235

⁹ Present Address: Pohang University of Science and Technology, Pohang, Korea 790-784

¹⁰ Present Address: Korea Institute of Standards and Science, P.O. Box 102, Yusong-Ku, Taejeon 305-600, South Korea

¹¹ Present Address: Center for High Energy Physics, Kyungpook National University, 1370 Sankyok-dong, Puk-ku, Taegu, 702-701 Korea

¹² Present Address: University of Colorado, Boulder, CO 80309

¹³ Present Address: Dipartimento di Chimica e Física per l’Ingegneria e per i Materiali, Università di Brescia and INFN sezione di Pavia

¹⁴ Present Address: Nat. Inst. of Phys. and Nucl. Eng., Bucharest, Romania

¹⁵ Present Address: Lucent Technology

¹⁶ Present Address: Adams State College, Alamosa, CO 81102

¹⁷ Present Address: Intel Corporation, Portland, 5200 N.E. Elam Young Parkway Hillsboro, OR 97124

The FOCUS detector (see Figure 1) is a large aperture spectrometer with excellent vertexing and particle identification. A photon beam is derived from the bremsstrahlung of secondary electrons and positrons with an ≈ 300 GeV endpoint energy produced from the 800 GeV/ c Tevatron proton beam. The charged particles which emerge from the target are tracked by two systems of silicon microvertex detectors. The upstream system, consisting of 4 planes (two views in 2 stations), is interleaved with the experimental target, while the other system lies downstream of the target and consists of twelve planes of microstrips arranged in three views. These detectors provide high resolution separation of primary (production) and secondary (decay) vertices with an average proper time resolution of ≈ 30 fs for 2-track vertices. The momentum of a charged particle is determined by measuring its deflections in two analysis magnets of opposite polarity with five stations of multiwire proportional chambers.

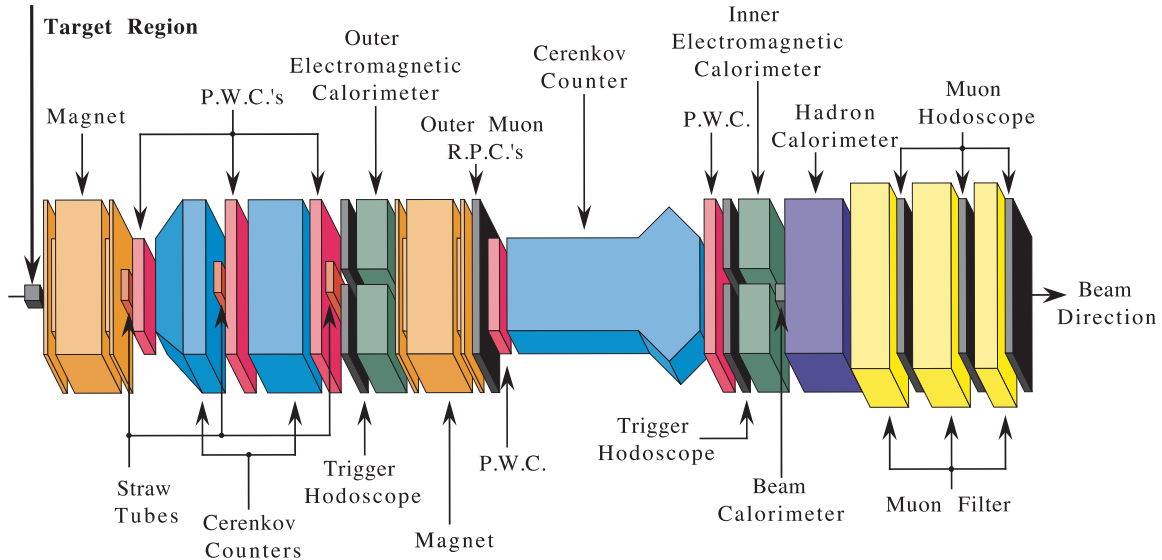


Fig. 1. A schematic drawing of the FOCUS spectrometer. The target region consists of a segmented BeO target, the interleaved target silicon planes, trigger counters, and the 12 plane silicon tracking array. The spectrometer is approximately 32 meters long.

2 The FOCUS Čerenkov system

Three multicell threshold Čerenkov counters are used to discriminate between electrons, pions, kaons, and protons. The Čerenkov system hardware was essentially unchanged from that used in E687 and is described in detail in Reference [1]. A brief description of the Čerenkov system follows.

There are three multicell threshold detectors in the experiment, referred to as C1, C2, and C3. The detectors are operated at atmospheric pressure and in the threshold mode. The gases are chosen so that different indices of refraction (*i.e.* different light velocities) establish different momenta in which pions, kaons, and protons will begin to radiate Čerenkov light (see Table 1). For our system the three pion thresholds were chosen to be 4.5, 8.4, and 17.4 GeV/ c by use of appropriate gas mixtures. The photoelectron yield ranged from roughly 2.5 to 20 depending on the phototube and Čerenkov counter.

The detector C1 is the most upstream of the three Čerenkov counters, lying just beyond the first analysis magnet, between the first two PWC's (multi-wire proportional chambers) P0 and P1. The gas used was a helium-nitrogen mixture, and the total length of the gas volume along the beam direction is 180 centimeters. The Čerenkov detector C2 has the lowest threshold of the three detectors with a pion threshold of 4.5 GeV/ c . The gas was pure N₂O, and the total length of the counter gas volume along the beam direction is 188 centimeters. The detector is located between P1 and P2.

The C1 and C2 Čerenkov counters can detect all charged tracks that are generally reconstructible in FOCUS. The 3rd Čerenkov detector C3 is located downstream of the second analysis magnet. Only higher momentum tracks make it through the aperture of this magnet, so C3 only helps in the identification of these tracks. The counter is a helium threshold counter which was 704 centimeters in length.

Table 1

Čerenkov counter specifications. The momentum threshold for the three most relevant charged particles and the Čerenkov cone radius for a $\beta = 1$ track at the image plane are given for each counter.

counter	Gas	Thresh (GeV/c)			No. Cells	Avg. PE	Čerenkov Radius (cm)
		pion	kaon	proton			
C2	N ₂ O	4.5	15.9	30.2	110	8 – 11	5.8
C1	He-N ₂	8.4	29.7	56.5	90	2.5 – 3.6	3.0
C3	He	17.4	61.5	117	100	9	5.6

3 The old versus new Čerenkov algorithm

While the Čerenkov hardware used in FOCUS was essentially the same as E687, a completely new Čerenkov algorithm was written for FOCUS. This new algorithm will be referred to throughout this article by the acronym CITADL (for Čerenkov Identification of Tracks by an Algorithm using Digital Likelihood). Before describing the new algorithm, we briefly describe the previous algorithm known as LOGIC. For a more complete description of this algorithm see reference [1].

Unlike CITADL, whose decision is based on the individual firing pattern of all 300 cells comprising the FOCUS/E687 Čerenkov system, LOGIC based its identification on the overall firing status of C1, C2, and C3. LOGIC rendered a single identification indicating whether or not the track was consistent with the electron, pion, kaon, and proton hypothesis.¹⁸ This decision was based on the track momentum and the Čerenkov light observed in the three threshold Čerenkov counters. A counter was declared “on” if any of the cells within the track’s Čerenkov cone fired. A counter was declared “off” if no cells within the cone fired and a minimum number of expected photoelectrons (typically 2.5) was expected under the pion hypothesis.¹⁹ Otherwise the firing status

¹⁸ Muons can only be effectively separated from pions over a narrow momentum range just below each counter’s pion threshold. Both E687 and FOCUS had a separate muon detection system to provide high quality muon identification.

¹⁹ In order to save time, LOGIC computed the expected number of photoelectrons

for that counter was declared unknown and its information was removed from the final decision. The observed on or off firing status was then compared to whether or not the counter should have fired under a given hypothesis. This prediction was based solely on whether or not the track momentum exceeded an “effective” momentum threshold for that hypothesis.²⁰

Although the LOGIC algorithm was very effective at helping to isolate charm particles in E687, it did have shortcomings. LOGIC tended to discriminate against pions when one required positive kaon and proton identification. Much of LOGIC’s tendency towards light particle identification was intended given the goal of strongly suppressing pion backgrounds to the kaons found in Cabibbo favored charm final states. For example, any cell firing within the Čerenkov cone sufficed to declare a counter on. But if no cells fired, a significant amount of predicted light was required before that counter would be declared off.

An unintended bias was due to accidental firings of the Čerenkov cells due to “noise.” The noise was due to RF noise on cables, tube noise, and light from untracked, charged particles such as electromagnetic spray and photon conversions produced in the very intense photon beam. The electromagnetic noise source could be very serious for Čerenkov cells located in the center of the system where occupancies sometimes approached 25–50%. Both effects tended to assign Čerenkov light to tracks making them inconsistent with “heavy” particles such as kaons and protons.

LOGIC’s tendency towards light particle identification both reduced the efficiency for kaon identification in Cabibbo favored decays and increased backgrounds for rarer Cabibbo suppressed decays such as $D^0 \rightarrow \pi^+\pi^-$ or $D^0 \rightarrow \pi^-\mu^+\nu$. In order to suppress the copious backgrounds from $D^0 \rightarrow K^-\pi^-$ or

for each cell under the pion hypothesis unless the track was under the pion threshold for the Čerenkov counter. If a track was below pion threshold, the light yield was computed under the electron hypothesis. This allowed the Čerenkov system to help in the identification of electrons.

²⁰ The “effective” threshold was slightly higher ($\approx 10\%$) than the actual threshold in order to crudely take into account the gradual rise in the expected light yield with momentum above threshold.

$D^0 \rightarrow K^- \mu^+ \nu$, one would typically require that the pion had a Čerenkov response which was inconsistent with that for a kaon.

While studying Cabibbo suppressed states, we used D^0 's skimmed from a sample of $D^{*+} \rightarrow D^0 \pi^+$ with no Čerenkov cuts to measure the fraction of kaons which passed the pion cuts. Typically 5% of kaons were misidentified as pions in E687 by the LOGIC Čerenkov algorithm. Because of the inflexibility of the LOGIC algorithm, one would need to redesign the internal cuts to minimize the misidentification of kaons as pions and re-run the algorithm from tapes that had the required Čerenkov ADC information. Although, in principle, LOGIC could be re-run with other internal cuts, that was not a practical option since data summary tapes typically did not contain the Čerenkov ADC information.

CITADL is primarily motivated by the desire to produce a more flexible Čerenkov identification algorithm than LOGIC. In fact, the overall performance of CITADL was significantly better than that of LOGIC, primarily because CITADL allows for the possibility of accidental firing of Čerenkov cells. Rather than making a hard decision, on whether or not a track was consistent with a given hypothesis, CITADL returned relative likelihoods that the track had a Čerenkov pattern similar to that expected for the electron, pion, kaon, or proton hypothesis. One could then, for example, put a minimum cut on the likelihood ratio that the kaon hypothesis is favored over the pion hypothesis in order get sufficiently clean kaons to do the required physics. Unlike LOGIC, very few cuts were required to be “hardwired” in the CITADL algorithm.

Like LOGIC, CITADL only uses the on/off status of Čerenkov cells rather than their pulse height in identifying particles. This decision made the computation of likelihoods simple since a cell's firing probability is given by the Poisson probability $(1 - \exp(-\mu))$ where μ is the expected number of photoelectrons under the given particle hypothesis.²¹

²¹ This assumes that the gains and thresholds are set such that a single photoelectron will produce an ADC count in excess of the threshold required to call a cell on. Under this assumption a cell will fire unless 0 photoelectrons are observed when μ are expected. The Poisson probability of getting zero photoelectrons is $\exp(-\mu)$.

CITADL constructed a log likelihood variable based on the firing probability for all Čerenkov cells that a given track could potentially affect all cells within the track’s $\beta = 1$ Čerenkov cone. Assuming for the moment, that a cell only fired in response to Čerenkov light, if the cell fired, and μ photoelectrons were expected, the log likelihood was incremented by $\log(1 - \exp(-\mu))$; while if the cell failed to fire the log likelihood was incremented by $\log(\exp(-\mu))$. Cells which were inside more than one track’s Čerenkov cone were considered “confused” and excluded from the sum. The likelihood returned by CITADL is similar in spirit to the traditional continuous likelihood used in fitting. The only difference is that each event has only two outcomes—on or off. For this reason, we call it a “digital” likelihood.

CITADL returns its identification in the form of χ^2 like variables which we will call W_e , W_π , W_K , and W_p . They are defined by $W_i = -2 \sum_j^{\text{cells}} \log P_j$ where P_j is the probability for the observed outcome (on or off) for the j 'th cell under each of the 4 particle hypotheses. One would typically require that potential charm decay kaons pass a minimum cut on a likelihood difference variable such as $\Delta W_K \equiv W_\pi - W_K$. A large ΔW_K implies that the kaon hypothesis is significantly favored over the pion hypothesis. Unlike the case in LOGIC, there is no need to introduce “effective” thresholds, since the μ dependence on momentum is explicitly taken into account. There is also no need to declare a minimum number of photoelectrons required for a Čerenkov decision. If a very small number of photoelectrons discriminated the two hypotheses, CITADL returns likelihood differences close to zero.

In computing the log likelihood, we take into account the probability that a given Čerenkov cell fires accidentally due to noise as well as firing due to a given track. We determined the accidental firing rate by measuring the fraction of times a Čerenkov cell would fire, even if it were outside of the $\beta = 1$ Čerenkov cone of all observed tracks. A typical plot of the accidental rate as a function of cell number for one of the runs is shown in Figure 2. The accidental rate varied considerably and for central cells was very large. It is very easy to incorporate accidental firing rates in the firing probability. The prescription is $P_{\text{fire}} = a + (1 - \exp(-\mu)) - a (1 - \exp(-\mu))$ where a and μ are the accidental rate and the number of photoelectrons expected for the given cell. We found that a was often proportional to the beam intensity—especially for cells near

the beam axis. CITADL included this effect as well. The inclusion of realistic accidental rates significantly improved the performance of our new algorithm relative to LOGIC.

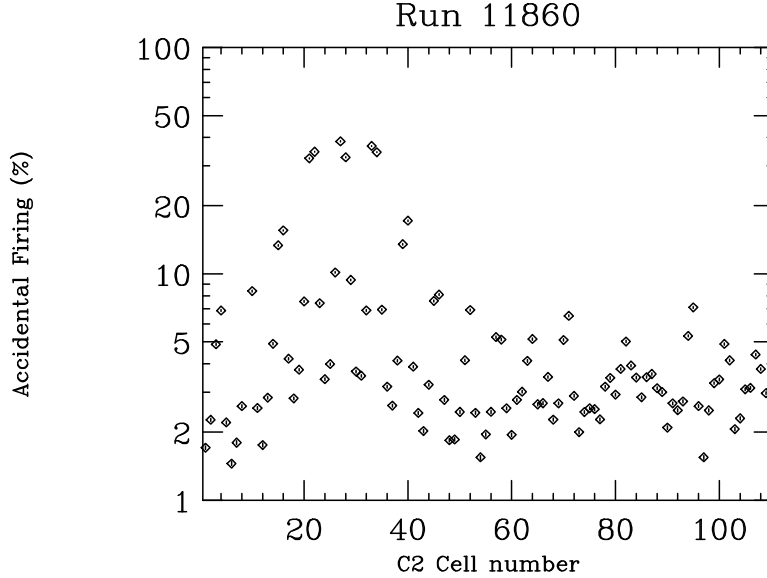


Fig. 2. The fraction of times (in percent) that a cell in C2 fires when no detected track’s $\beta = 1$ Čerenkov cone impinges on the cell. These data were accumulated over a single run. Although most of the cells have an accidental rate of a few percent, cells located near the beam axis have accidental rates as high as 40%.

4 CITADL Performance

The very high statistics FOCUS data set provided numerous checks of the performance of the Čerenkov system and the CITADL algorithm – often on a run-by-run basis. These checks used decays into final states of known daughters. The decays $K_S \rightarrow \pi^+\pi^-$ provided a very pure and highly copious source of pions, consisting of 15,000 decays in each of our nearly 6000 runs. This sample was large enough to provide an accurate photoelectron re-calibration for nearly all of the 300 cells in the Čerenkov system.

Although not nearly as copious as our K_S sample, the decay $\Lambda \rightarrow p\pi^-$ provided a clean sample of proton and low momentum pion decays.²² Finally the decay

²²Reference [2] describes the method used to reconstruct the K_S and Λ topologies

$\phi \rightarrow K^+K^-$ was used to measure the Čerenkov identification of kaons on a run-by-run basis.²³ The run-by-run fraction of misidentified daughters from the K_S, Λ , and ϕ decays for several Čerenkov cuts was used as a stability monitor of the Čerenkov system. Figures 3 and 4 show examples of these “misidentification” monitors.

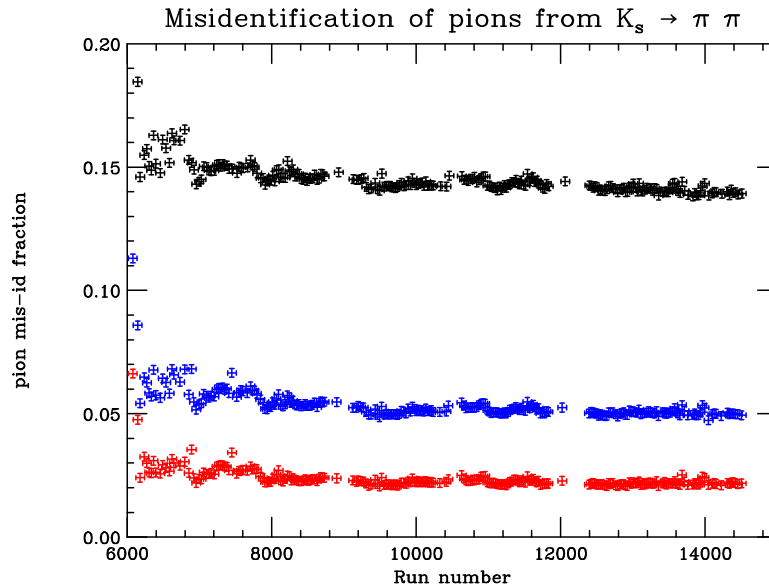


Fig. 3. The fraction of times that a pion from $K_S \rightarrow \pi^+\pi^-$ is misidentified as a kaon, proton, or electron for three different CITADL cuts. Each point is averaged over 25 runs.

We also found that it was possible to use golden mode charm as a monitor of Čerenkov performance. Figure 5 shows a 405,000 event golden mode charm sample obtained (using about 75% of our data) without any Čerenkov cuts. A selection of cuts on vertex detachment, isolation, the $D^{*+} - D^0$ mass difference, and momentum were used to obtain this reasonably clean sample. Also shown are sideband regions used for background subtraction. Figure 6 shows the likelihood difference $\Delta W_K = W_\pi - W_K$ for the kaon and pion daughters from these background subtracted charm decays for tracks with two ranges of momentum. For convenience, we will call the variable $\Delta W_K \equiv W_\pi - W_K$ “kaonicity”. A positive kaonicity implies that a given track is more likely to be a kaon as opposed to a pion.

in FOCUS.

²³ To obtain a clean enough ϕ sample to make a meaningful background subtraction, we required that one of the two kaons was Čerenkov identified.

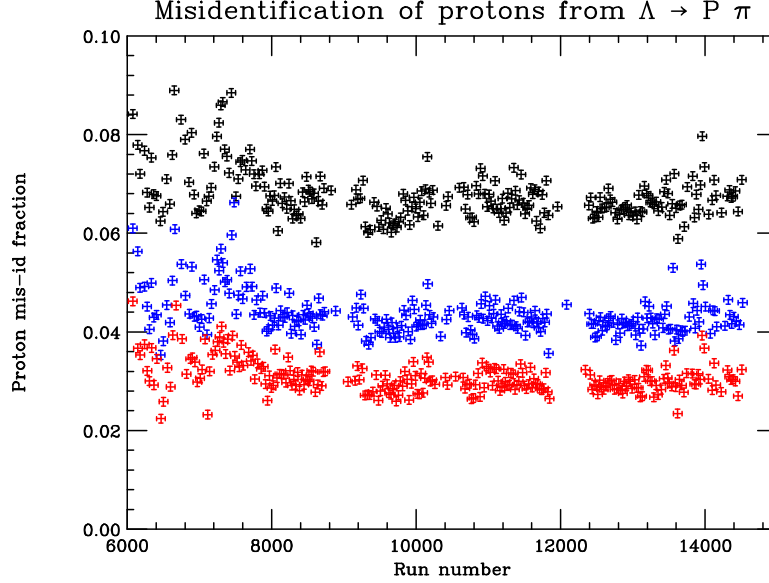


Fig. 4. The fraction of times that a proton from $\Lambda \rightarrow p\pi^-$ is misidentified as a light particle for three different CITADL cuts. Each point is averaged over 25 runs.

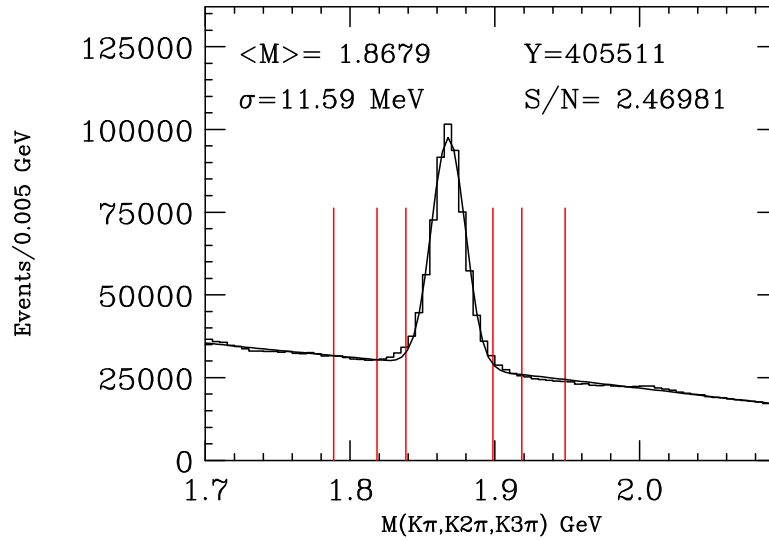


Fig. 5. Invariant mass plot for the three golden mode decays $D^0 \rightarrow K^- \pi^+, K^- \pi^+ \pi^+ \pi^-$, and $D^+ \rightarrow K^- \pi^+ \pi^+$. The reconstructed D^+ mass was shifted by $5 \text{ MeV}/c^2$ so that its peak will reconstruct in the same place as the peak of the D^0 . This data has vertex quality and kinematic cuts only. No Čerenkov cuts were used. The vertical lines denote signal and sideband regions which will be used to make a background subtraction.

Figure 6(a) shows the kaonicity distribution for charm kaons and pions in a momentum range above the pion threshold of C2 (the lowest threshold counter)

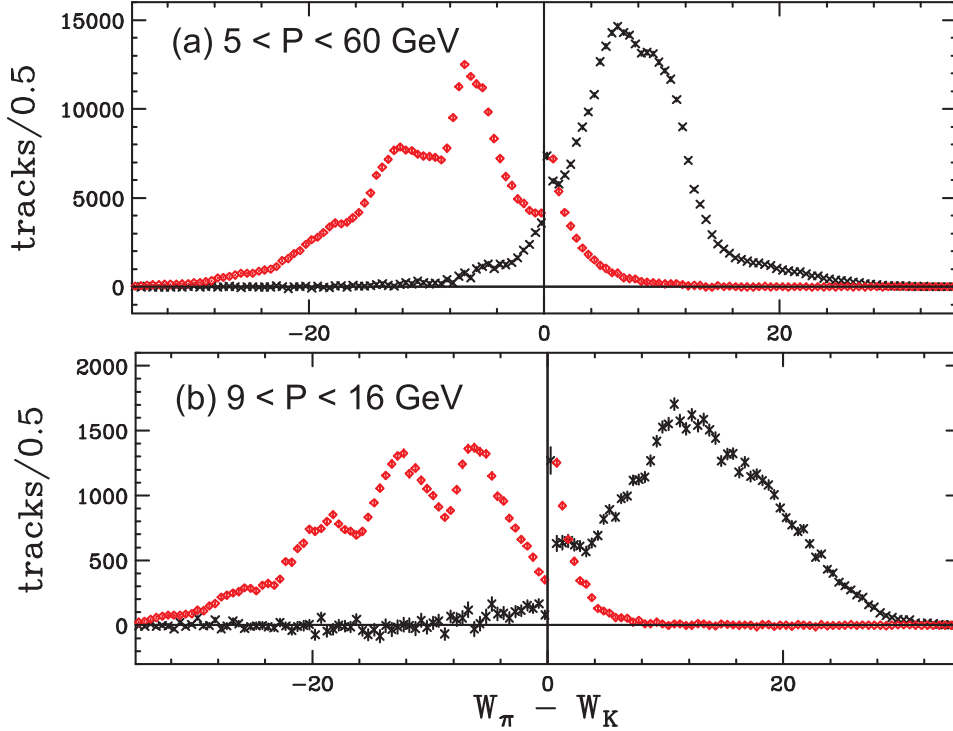


Fig. 6. The log likelihood difference $W_\pi - W_K$ distribution obtained from background subtracted kaons (x's) and pions (diamonds) from the golden mode charm signal shown in Figure 5. The pion distributions were rescaled to have the same area as the kaon distributions. Fig. (a) Tracks with momenta in the range $5 < P < 60$ GeV/c. Fig. (b) Tracks with momenta in the range $9 < P < 16$ GeV/c. There are off scale spikes in the 0-bin consisting of 20,000 and 4,500 events for Fig. (a) and (b).

but below the kaon threshold of C3 (the highest threshold counter). Outside of this momentum range, the FOCUS Čerenkov system is incapable of much K- π separation and the kaonicity distribution is strongly peaked near zero.²⁴ Figure 6(b) shows the kaonicity distribution in the more restricted range from 9 to 16 GeV/c. In this range kaon-pion discrimination is particularly effective since it lies above the pion threshold for C1 but below the kaon threshold of C2.

Figure 6 shows that, even though the likelihoods are constructed from the dis-

²⁴ CITADL offers some slight K- π discrimination outside of this range since it can exploit the momentum dependence of photoelectron yield beyond the C3 kaon threshold: *i.e.* the threshold is not infinitely sharp.

crete firings of Čerenkov cells, the kaonicity distribution for kaons is reasonably continuous except near $\Delta W_K = 0$. As Figure 6(a) shows, averaged over the accepted charm momentum spectrum, pion backgrounds to kaons can be very effectively eliminated while still maintaining high efficiency for charm kaons. A cut just above kaonicity of zero rejects a large fraction of pions. The fraction of background pions dies away exponentially with the kaonicity cut above zero. Over the more restricted range from 9 to 16 GeV/ c , where cells from both C1 and C2 discriminate pions from kaons, the ΔW_K distribution shows a significantly larger average kaonicity. One can make a very stringent kaonicity cut to suppress pion backgrounds and still maintain good efficiency for real kaons.

The situation for pion identification is essentially the mirror image of that for kaons. The contamination of kaons into the $\Delta W_K < 0$ region falls off exponentially in ΔW_K , while the pion spectrum extends below $\Delta W_K < -20$. In the region from 9 to 16 GeV/ c , where both C1 and C2 discriminate pions from kaons, the average kaonicity of pions becomes significantly more negative permitting one to make more stringent cuts to reduce misidentification.

4.1 *Understanding the kaonicity distributions*

We begin by discussing the kaonicity distribution for kaons in Figure 6. As described below, we use a simplified²⁵ model to conclude that the positive half of the kaonicity distribution is controlled by twice the total number of photoelectrons in those Čerenkov cells which discriminate pions from kaons and the negative half of the spectrum depends on the accidental firing rate but is damped exponentially in kaonicity.

When a track is assigned a non-zero kaonicity, there are some Čerenkov cells that would be expected to fire if the track were a pion and would be expected

²⁵ One simplification is that the model assumes that all pion-kaon discrimination in CITADL is due to cells which have pion thresholds below the track's momentum but kaon thresholds above the track's momentum. In fact there is extra discrimination for cells with kaon thresholds below the track momentum since the probability that the cell will fire under the kaon hypothesis is less than the firing probability under the pion hypothesis.

to fail to fire if the track were a kaon. If $\Delta W_K > 0$, these “discriminating” cells did not fire. Let μ be the sum of the photoelectrons expected for pions for these “discriminating” cells. Assuming a small accidental rate, the probability that these cells would fail to fire under the kaon hypothesis is essentially 1, and under the pion hypothesis is $\exp(-\mu)$. The kaonicity is defined in terms of the probability that the light pattern agrees with the kaon hypothesis divided by the probability that the pattern agrees with the pion hypothesis or $\Delta W_K = -2 \log(P_\pi/P_K)$. After inserting these non-firing probabilities, we have $\Delta W_K = 2\mu$. According to this model, the maximum kaonicity of ≈ 30 means that the FOCUS Čerenkov system provides at most 15 photoelectrons which discriminate between kaons and pions. In the momentum region between 9 and 16 GeV/ c , Figure 6(b) shows that the yield of discriminating photoelectrons is much larger than over the full range from 5 GeV/ c to 60 GeV/ c . This is because pions with momenta in this range should fire the cells of both C1 and C2 whereas kaons should not. The photoelectron yield for $\beta = 1$ tracks in C2 is typically in excess of 11—larger than that for C1 or C3.

If CITADL assigns a track $\Delta W_K < 0$, there must be discriminating cells which fired making the pion hypothesis more likely than the kaon hypothesis. For real kaons, such as those displayed in Figure 6, this can only happen due to accidental firing. Denote the probability that noise fires a discriminating cell by a . In the limit where there is a reasonable number of discriminating photoelectrons, the probability that the cells will fire under the pion hypothesis will approach 1. Hence if a cell accidentally fires for a kaon, CITADL will report a kaonicity of $\Delta W_K = -2 \log(P_\pi/P_K) = 2 \log(a)$ where a is the accidental firing rate. The probability that a kaon track will actually fire a discriminating cell will of course be $a = \exp(\Delta W_K/2)$. One therefore expects the roughly exponential fall off in negative kaonicity for real kaons which is observed in Figure 6.²⁶ To summarize, a positive kaonicity value is essentially twice the number of photoelectrons which discriminate kaons from pions at the momentum of the kaon; while the negative half depends on the distribution of accidental

²⁶ The distribution of negative kaonicities for kaons also depends on the distribution of noise rates for cells in the Čerenkov system. Deviations from an $\exp(\Delta W_K/2)$ distribution are therefore expected since the distribution of accidentals is nonuniform as shown in Figure 2.

firing rates and is suppressed by a factor of $\exp(\Delta W_K/2)$.

We next turn to a discussion of the ΔW_K distribution obtained for the pions shown in Figure 6. For negative kaonicities ($\Delta W_K < 0$), the kaonicity distribution exhibits considerable structure but when $\Delta W_K > 0$ it dies exponentially with kaonicity. The exponential fall-off in the $\Delta W_K > 0$ region is due to discriminating cells not firing for the pion thus causing CITADL to prefer the kaon hypothesis. For pions, this should happen with a probability of $P_\pi = \exp(-\mu)$ while for kaons it will occur with $P_K = 1$. Such tracks will therefore be assigned a kaonicity of $\Delta W_K = -2\log(P_\pi/P_K) = 2\mu$. We thus expect a kaonicity distribution for $\Delta W_K > 0$ given by the product of the spectrum of discriminating photoelectrons times the probability of the pion not firing the discriminating cells. This leads to a nearly exponential distribution since the probability of a pion not firing the discriminating cells is given by: $\exp(-\mu) = \exp(-\Delta W_K/2)$. In fact, the kaonicity spectrum of pions in the region $0.5 < \Delta W_K < 10$ is well fit to the form $\exp(-0.4 \Delta W_K)$.

We next consider the $\Delta W_K < 0$ half of the kaonicity spectrum for pions. In this region, the pion hypothesis is favored over the kaon hypothesis if the discriminating cells fired. Assuming a relatively large number of discriminating photoelectrons, the probability the cells will fire is close to $P_\pi = 1$. Under the kaon hypothesis the cells would only fire due to accidentals which would occur with a probability of $P_K = a$. The pion would then be assigned a kaonicity of $\Delta W_K = -2\log(P_\pi/P_K) = 2\log(a)$. If several discriminating cells fire, the kaonicity distribution will be incremented by several multiples of $2\log(a)$. Indeed several peaks are present in the $\Delta W_K < 0$ spectrum of Figure 6(b) which appear at multiples of approximately 6.25 which implies a typical accidental rate of $a = \exp(-6.25/2) = 0.044$. This estimated a is consistent with the typical accidental rate shown in Figure 2.

To summarize, the $\Delta W_K > 0$ spectrum for pions is controlled by the number of discriminating photoelectrons and is damped by a Poisson inefficiency factor of $\exp(-\Delta W/2)$ while the $\Delta W_K < 0$ region is controlled by multiples of twice the log of the accidental firing rate.

This model, among other things, explains why the pion-kaon separation in the

momentum range of Figure 6 (b) is so much better than over the complete momentum spectrum. Because C1 and C2 both discriminate in this narrow momentum range, there are more Čerenkov cells available to discriminate between the pion-kaon hypothesis. Hence there are more discriminating photoelectrons which increases the average kaonicity for kaons, and more multiples of $-2 \log(a)$ which further decreases the (negative) kaonicity distribution for pions.

4.2 Using Čerenkov Information to Reduce Charm Backgrounds

As Figure 5 shows, it was indeed possible to get reasonably clean charm signals without the use of Čerenkov information. However, many FOCUS analyses employed Čerenkov cuts as an effective way of increasing signal to noise, while maintaining reasonable efficiency. Figure 7 illustrates the effectiveness of kaon and pion Čerenkov cuts for $D^0 \rightarrow K^- \pi^+ \pi^+ \pi^+$ events selected by requiring that the secondary to primary vertex detachment exceeded 9 standard deviations. No Čerenkov cuts were used in the initial selection. The kaon cut is on “kaonicity” or the log likelihood difference $\Delta W_K \equiv W_\pi - W_K$ discussed previously. The pion cut is based on a pion consistency variable which we will call “piconicity” or $\Delta W_\pi \equiv W_{\min} - W_\pi$, where W_{\min} is smallest negative log likelihood of the 4 particle hypotheses. The ΔW_π cut is placed on all D decay pions and is meant to ensure that no pion being considered as a charm daughter is grossly inconsistent with the pion hypothesis.²⁷ A cut such as $\Delta W_\pi > -2$ means that none of the other 3 particle hypotheses is favored over the pion hypothesis by more than a factor of $\exp(2/2) = 2.71$. For the $D^0 \rightarrow K^- \pi^+ \pi^+ \pi^+$ sample the requirement that $\Delta W_K > 0$ preserves 84% of the yield while increasing the signal to noise by a factor of 6.2. The more stringent $\Delta W_K > 2$ and $\Delta W_\pi > -2$ preserves 75% of the uncut signal yield but increases the signal to noise by a factor of 16.

²⁷ We generally use a consistency cut rather than demanding that the pion is favored over both the kaon and electron hypothesis since the momentum range at which pions can be distinguished from electrons is below 17 GeV/ c for tracks traversing all three Čerenkov counters and below 8.5 GeV/ c for 3 chamber pions which traverse only C1 and C2.

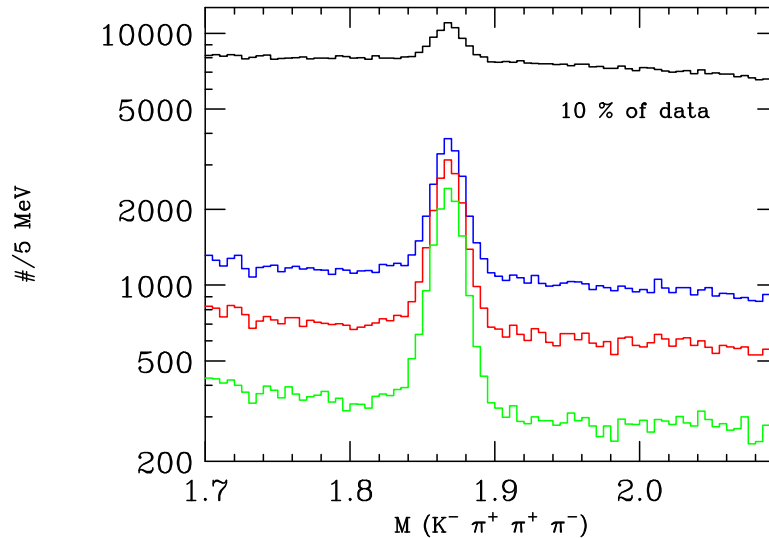


Fig. 7. Illustration of the effectiveness of Čerenkov cuts in reducing backgrounds to $D^0 \rightarrow K^- \pi^+ \pi^+ \pi^-$. Note the logarithmic scale. The upper curve has no Čerenkov cuts. The second histogram requires $\Delta W_K > 0$. The third requires $\Delta W_K > 2$. The fourth histogram requires $\Delta W_K > 2$ and $\Delta W_\pi > -2$. A considerable improvement in the signal to noise is evident with only moderate loss in efficiency. The fitted signal yields in these plots are 15307, 12783, 11699, and 9996 respectively.

One of the goals of the CITADL algorithm was to be much more efficient than LOGIC in suppressing the number of kaons which are misidentified as pions to enable us to more effectively study Cabibbo suppressed decays. An example of such a process is the $D^0 \rightarrow \pi^+ \pi^-$ which is plagued by a large background from misidentified $D^0 \rightarrow K^+ \pi^-$ decays which occur with a branching ratio that is approximately 25 times larger than that of $D^0 \rightarrow \pi^+ \pi^-$. Figure 8 compares the dipion mass spectrum from the published E687 signal to a version from half of the FOCUS data set. The E687 sample used LOGIC. The FOCUS sample required $W_K - W_\pi > 3$ for both pions in order to significantly reduce $D^0 \rightarrow K^+ \pi^-$ contamination. Much of the improvement in event yield is due to the fact that FOCUS took roughly a factor of 15 times the E687 data set. We have also required that the dipion vertex be outside of the FOCUS target material to further increase our signal to noise relative to E687. However, the CITADL algorithm is responsible for the significant reduction in FOCUS data of the reflection from misidentified $D^0 \rightarrow K^+ \pi^-$ relative to the $D^0 \rightarrow \pi^+ \pi^-$ signal compared to what was achievable in E687.

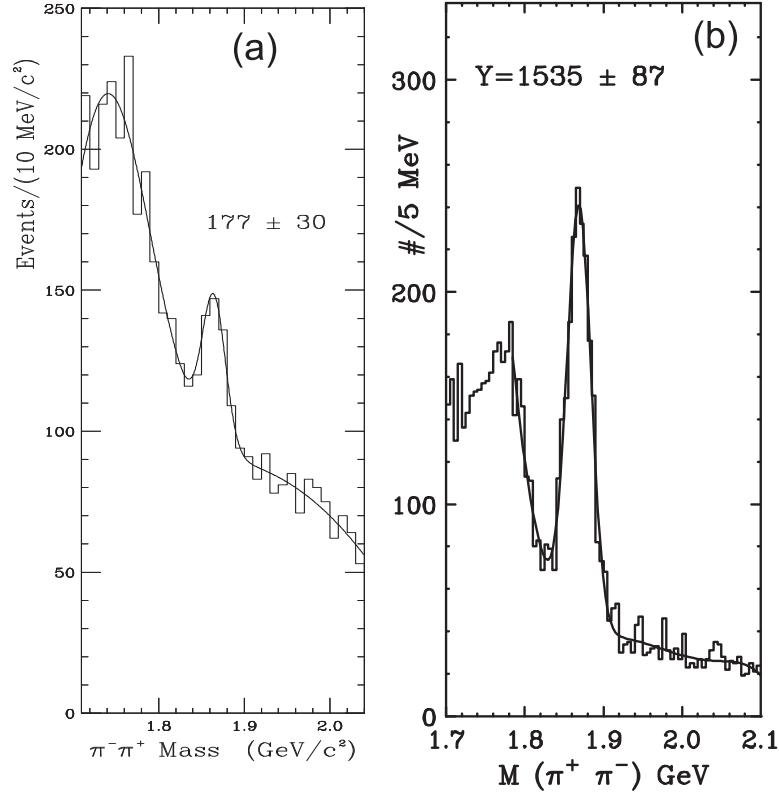


Fig. 8. (Left) E687 signal for $D^0 \rightarrow \pi^+\pi^-$ from Reference [3]. The massive distortion in the background at lower masses is due to contamination from misidentified $D^0 \rightarrow K^+\pi^-$. (Right) FOCUS signal for $D^0 \rightarrow \pi^+\pi^-$ from half of our data set.

Figure 9 is an example of a plot used to gauge the effectiveness of a set of Čerenkov cuts on the pions and kaons from a very small sample of $D^+ \rightarrow K^-\pi^+\pi^+$ decays. The data satisfied our standard skim cuts for this mode: a good quality vertex intersection ($\text{CL} > 1\%$), a kaonicity cut of $\Delta W_K > 0.5$, and a secondary to primary detachment exceeding 2.5 standard deviations ($\ell/\sigma > 2.5$). This particular plot used the sample of D^+ decays which verticized outside of the target material and target microstrip system to remove backgrounds from multiple interactions. We show the yield versus signal to noise for 2 detachment cuts, and a sequence of Čerenkov cuts on the kaons and pions.²⁸ Figure 9 shows that the “piconicity cut” is essentially as effective

²⁸ Both the yields and signal to noise were based on fits to a Gaussian signal over a polynomial background. We define the signal to noise ratio as the ratio of the fitted number of signal events at the peak over the fitted number of background events at the peak mass.

a cut as the kaonicity cut. Figure 9 also shows that the Čerenkov cuts increase the signal to noise by a nearly constant factor at the two detachment cuts being considered.

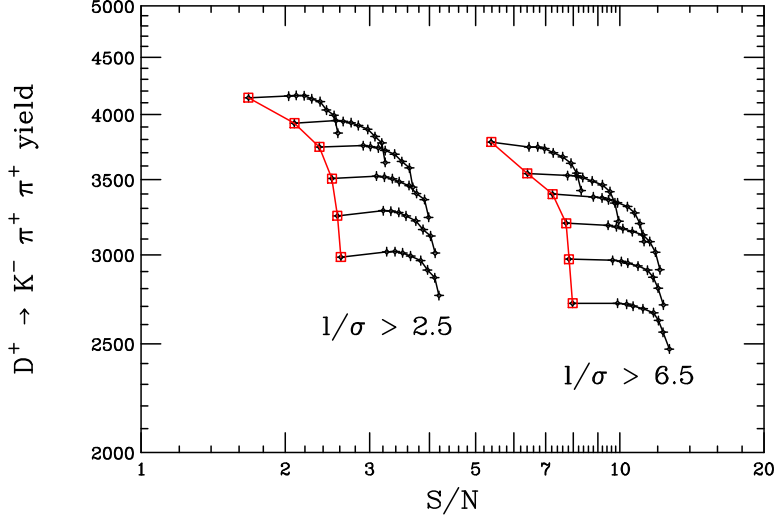


Fig. 9. Illustration of the effectiveness of Čerenkov cuts in reducing backgrounds to $D^+ \rightarrow K^- \pi^+ \pi^+$ which verticize outside of the target microstrips and target material. We form a “cut tree” by plotting the signal yield versus S/N for two different detachment cuts and several cuts on kaonicity and pion consistency (piconicity). The kaonicity cuts (the main trunks) range from $\Delta W_K > 0.5, 1, 2, 3, 4, 5$. The piconicity cuts (the branches) are “no cut”, $\Delta W_\pi > -10, -9, \dots, -3$. Only 2 % of the our complete data was used for this plot.

5 Calibration and Monitoring

We made a large number of plots while reconstructing our data to monitor Čerenkov system performance. Examples of such plots which we have already discussed include Figures 2, 3, and 4 which serve as monitors of accidental rates, and Vee (K_S or Λ) daughter misidentification. We found that our most powerful calibration tool used pions from $K_S \rightarrow \pi^+ \pi^-$ since roughly 15,000 clean K_S 's were reconstructed during each of our ≈ 6000 data runs. These pions were used to study how well we could predict the firing rate for cells. An example of such a study is shown in Figure 10 which plots the observed average firing rate versus the predicted. These particular plots are summed over all

cells in each Čerenkov counter. They represent the statistics on a single run. The prediction depends on the assumed cell geometry, the accidental firing rates, the relative quantum efficiency of each tube, and the validity of the analytic model used to quickly compute the fraction of Čerenkov light falling within the cell boundary. This model was known to have problems for cells on the planar mirror boundaries of C1 and the planar mirror apex of C2. It is clear from Figure 10 that the light predictions were imperfect. We believe that the impact of these imperfections was slight on overall Čerenkov identification.

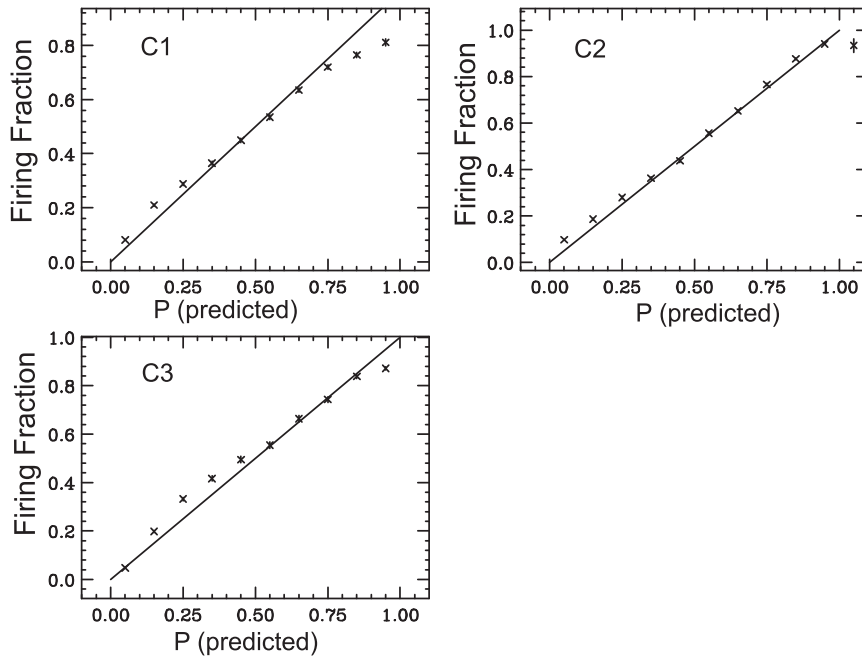


Fig. 10. Plots of the actual firing rate as a function of the predicted firing rate for all cells within the given counter. We use pions from the decay $K_S \rightarrow \pi^+\pi^-$. This set of plots was obtained in run 13955.

We worked diligently to insure that CITADL used good information on the performance of each of the 300 cells comprising the FOCUS Čerenkov information. The two critical ingredients are the photoelectron yield for a $\beta = 1$ track and the “accidental” firing rate. We found that the performance of some photomultipliers varied significantly during the 12 month run. Occasionally this was due to the maintenance of the Čerenkov system, such as changing bases and phototubes. More often, small shifts in the ADC pedestals would create a dramatic apparent increase in the “noise” level of the tube, which could be easily corrected by raising the minimum ADC count required by CITADL

to call a cell “on.” Although special calibration runs were taken in order to understand the Čerenkov system, we found that the best monitoring of the Čerenkov system was obtained through regular data taking. In this section, we describe some of these *in situ* calibration and monitoring methods.

5.1 Photoelectron Calibration and Monitoring

We developed a powerful way of monitoring the photoelectron yield as a function of time for nearly all of the 300 cells comprising the FOCUS Čerenkov system. This calibration method fit for the $\beta = 1$ photoelectron yield of each cell by minimizing CITADL likelihood W_π for pions from $K_S \rightarrow \pi^+\pi^-$. The W_π was incremented for each K_S pion daughter that was predicted to leave at least 0.1 photoelectron in a given cell. The likelihood was incremented using background subtraction weight of 1 if the K_S mass was in the signal region and -1 if the mass fell in symmetrically placed, half width sidebands. Separate $\sum W_\pi$ sums were computed for different assumed $\beta = 1$ photoelectron yields for the given cell which ranged from 20% to 160% of the nominal photoelectron yield. Typical log likelihood versus photoelectron ratio plots obtained in a single run are shown in Figure 11. With the statistics available in a single run one could get an adequate re-calibration of the inner Čerenkov cells which are struck most often.

As a stability monitor, we also summed the W_π from all of the K_S pions in a given run over all of the cells in our three Čerenkov counters. The minima of these grand likelihoods are plotted as a function of run number in Figure 12 and give an overall scale factor for each of the three counters. Apart from some photoelectron fluctuations unique to C1 in the early running, Figure 12 shows that the average photoelectron yield from all three Čerenkov counters tended to fluctuate together in a way which we learned was correlated with changes in barometric pressure.

PE calibration for run 13955

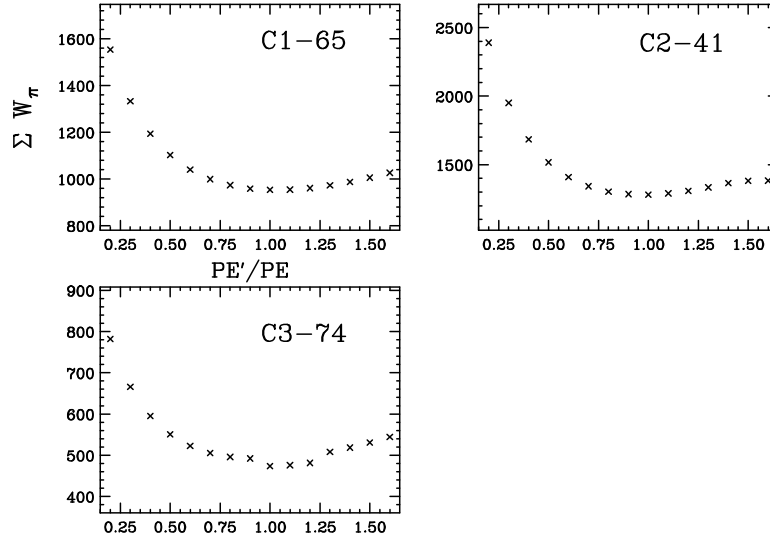


Fig. 11. Calibration curves for three cells in the Čerenkov system. We plot $\sum W_\pi$ for pion daughters from background subtracted $K_S \rightarrow \pi^+\pi^-$ decays which strike the cell summed over all such pions in run 13955. This likelihood is computed for 15 assumed photoelectron ratios relative to the $\beta = 1$ yield used by CITADL. The example cells are in the inner section of each Čerenkov counter

5.2 Noise Calibration and Monitoring

CITADL makes direct use of the observed accidental firing rate for Čerenkov cells which is generally $\approx 2 - 5\%$ for most cells but can be quite high ($\approx 40\%$) for cells close to the beam axis. We believe much of this noise for central cells is due to the high rate of e^+e^- pairs that accompany our hadronic photoproduced events. Most of the very “noisy” cells showed an accidental rate which was roughly proportional to the instantaneous beam intensity. Figure 13 illustrates this point for two Čerenkov cells. A few words are in order. As a measure of the accidental rate, we use a variable called the “Poisson Accidental Rate”. This “Poisson” rate (μ_a) is related to the accidental rate a (or fraction of times a cell fires when no track is pointing at it) via $1 - \exp(-\mu_a) \equiv a$. We assumed in our treatment that μ_a rather than a was linear in the beam intensity.²⁹ We found that the average number of embedded pair tracks per triggered

²⁹ For small a , $a \approx \mu_a$ but clearly as $a \rightarrow 1$, a cannot continue to grow linearly with intensity.

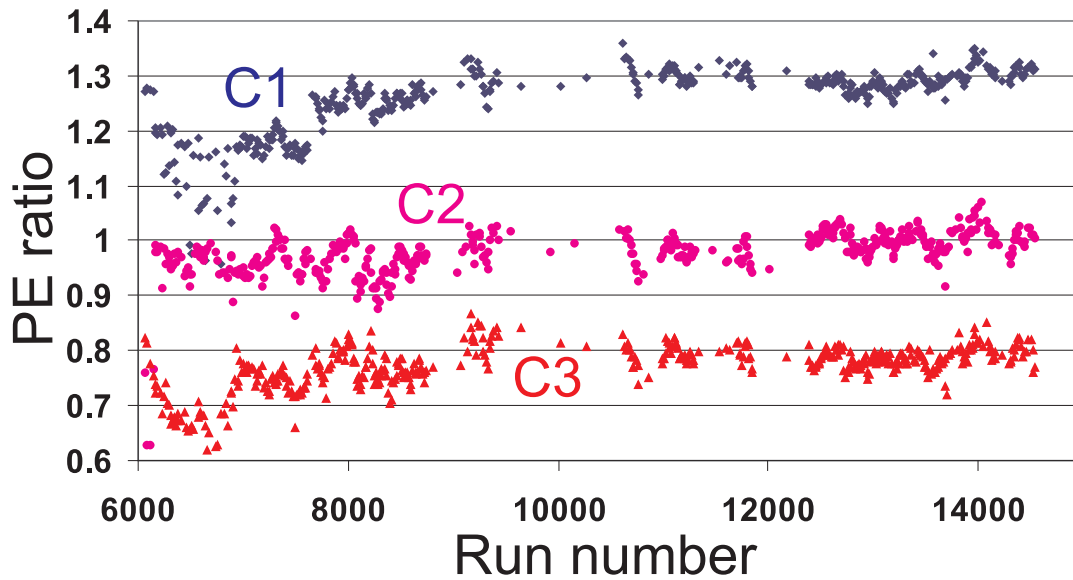


Fig. 12. Plot of the relative photoelectron yield for all three counters as a function of run number. Each point is a 10 run average and the data for each counter are offset vertically for clarity. The photoelectron yield relative to that assumed in the calibration is always within 20% of unity until run 9000 and within 10% thereafter.

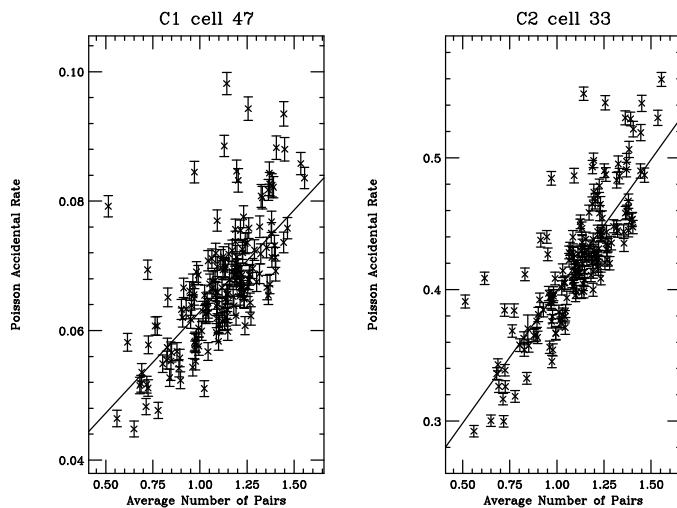


Fig. 13. Plots of Poisson accidental rate versus instantaneous beam intensity for two Čerenkov cells.

event formed a very convenient monitor of our average instantaneous beam intensity. Embedded pair tracks are from a Bethe-Heitler beam conversion which happen to lie within the resolving time of the chambers and microstrips when triggered by one of our event triggers. Pair tracks are easy to identify

since they are consistent, within their expected multiple scattering, with being produced along the beam axis.³⁰

We found that the average number of pair tracks in coincidence with an event trigger was a good measure of the instantaneous beam intensity which included the sometimes dramatic effects of spill non-uniformity. We used linear fits of the Poisson accidental rate versus \langle pair tracks \rangle , such as those in Figure 13, to model the noise response for each of the 300 Čerenkov cells. Often several parameterizations were made for a given cell to cover run dependent changes in the accidental rate.

In fact the beam intensity varied significantly between the spills and even within a spill.³¹ To optimize Čerenkov algorithm performance, we devised a method to estimate the beam intensity directly before each recorded event and use this intensity measurement to estimate the accidental rate for each cell. This method used several scalers which were recorded on our raw event tapes during each second level, event trigger. One of these scalers counted the accelerator RF clock, the others counted the hits in two scintillation counters used in the first level trigger. The scalers were effectively reset each time we read an event out. The time rate of change of either of these two scintillation counters formed a direct measurement of the beam intensity right before the actual event. Figure 14 shows that both the average number of embedded pair tracks, and the accidental Čerenkov cell firing rates are strongly correlated with the scaler derived beam intensity even within a single spill of Run 7185.

6 Summary and Conclusions

In this article we describe a likelihood based Čerenkov algorithm used to identify charged particles in the FOCUS charm photoproduction experiment.

³⁰ The average number of embedded pair tracks was ≈ 1 per event throughout much of the FOCUS running owing to our very high intensity.

³¹ Typically we had one spill of protons every minute which lasted for about 20 seconds. The first 500 microseconds of this spill was “fast” extraction for neutrino experiments. A typical run lasted 40 minutes.

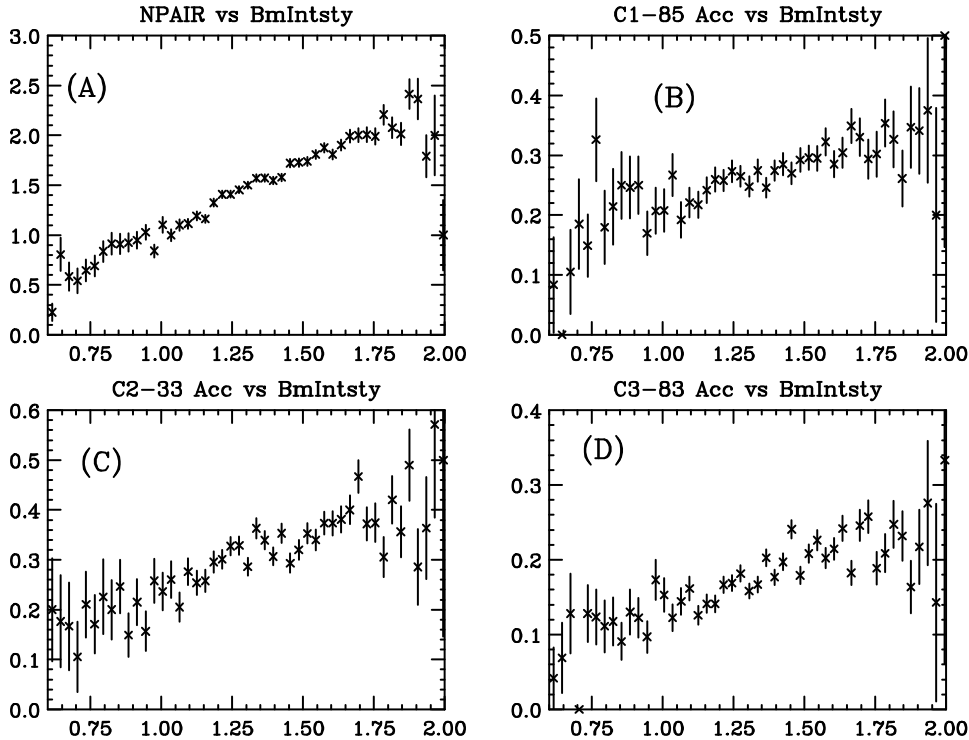


Fig. 14. Rate dependences of several quantities versus the scaler deduced intensity monitor within a single accelerator spill. Figure (a) shows the average number of embedded pair tracks versus the beam intensity. Figures (b), (c), and (d) show the accidental rate in three Čerenkov cells versus the beam intensity.

FOCUS used three multicell Čerenkov counters, operating in threshold mode. We believe that this algorithm may prove useful in future experiments employing threshold Čerenkov counters in high rate environments. This article describes the CITADL algorithm, illustrates its effectiveness on charm signals, and discusses the method we used for continuous monitoring of each cell’s photoelectron yield and noise.

Although the pulse heights for all of the firing Čerenkov cells in a given event were recorded, our algorithm did not use this pulse height information. The CITADL algorithm was based on the probability that Čerenkov cells uniquely associated with a given track either fired or failed to fire. Because there were only two outcomes per Čerenkov cell, we say the algorithm returned a “digital likelihood” for a given particle hypothesis. Given the large number of cells with different accidental rates and photoelectron yields comprising the FOCUS Čerenkov system, the “digital” likelihood provided an essentially continuous

identification variable.

By using only the on/off status of the Čerenkov cells, we found that it was possible to include the effects of “accidental” firing due (in our case) to the untracked electromagnetic debris in regions close to our photon beam. Essentially we combined the probability of a cell firing due to Čerenkov light, with an accidental firing probability using De Morgan’s Law. The accidental probability for each Čerenkov cell was parameterized in terms of an intrinsic accidental rate and a contribution proportional to the instantaneous beam intensity. By realistically including the accidental rate in our likelihood, we substantially improved our ability to identify light particles (such as pions) over the less sophisticated algorithm used in our previous charm photoproduction experiment, E687. Interestingly enough, the ability to positively identify pions with high efficiency and low kaon contamination, proved useful in significantly increasing our signal to noise even in Cabibbo favored charm decays.

The goal of the CITADL algorithm was to provide flexible identification with a broad efficiency versus misidentification curve. The flexibility of this algorithm has proven very useful in assessing systematic errors due to misidentified charm reflections in our recent studies of Cabibbo suppressed and doubly suppressed charm decays.[4]-[6]

We wish to acknowledge the assistance of the staffs of Fermi National Accelerator Laboratory, the INFN of Italy, and the physics departments of the collaborating institutions. This research was supported in part by the U. S. National Science Foundation, the U. S. Department of Energy, the Italian Istituto Nazionale di Fisica Nucleare and Ministero dell’Università e della Ricerca Scientifica e Tecnologica, the Brazilian Conselho Nacional de Desenvolvimento Científico e Tecnológico, CONACyT-México, the Korean Ministry of Education, and the Korean Science and Engineering Foundation.

References

- [1] E687 Collab., P. L. Frabetti *et al.*, Nucl. Instrum. Methods Phys. A 320 (1992) 519.

- [2] FOCUS Collab., J. M. Link *et al.*, Submitted to Nuclear Instruments and Methods.
- [3] E687 Collab., P. L. Frabetti *et al.*, Phys. Lett. B321 (1994) 295
- [4] FOCUS Collab., J. M. Link *et al.*, Phys. Lett. B485 (2000) 62
- [5] FOCUS Collab., J. M. Link *et al.*, Phys.Lett.B491 (2000) 232
- [6] FOCUS Collab., J. M. Link *et al.*, Phys.Rev.Lett. 86 (2001) 295